Korean J. Chem. Eng., 40(6), 1497-1509 (2023)
DOI: 10.1007/s11814-022-1368-9

pISSN: 0256-1115
eISSN: 1975-7220

Zinc oxide-tungsten oxide (ZnO-WO_3) composite for solar light-assisted degradation of organic dyes

Fatima Aziz*, Al-Zoha Warsi*, Hamoud H. Somaily,***, Muhammad Imran Din****, Humera Sabeeh*, Muhammad Farooq Warsi*,†, and Imran Shakir*****,†**

*Institute of Chemistry, Baghdad-ul-Jadeed Campus, The Islamia University of Bahawalpur, Bahawalpur 63100, Pakistan
**Research Center for Advanced Materials Science (RCAMS), King Khalid University, Abha 61413, P.O. Box 9004, Saudi Arabia
***Department of Physics, Faculty of Science, King Khalid University, P.O. Box 9004, Abha, Saudi Arabia
****School of Chemistry, University of the Punjab, New Campus, Lahore 54590, Pakistan
*****Department of Materials Science and Engineering, University of California, Lose Angles, United States of America
(*Received 11 August 2022 • Revised 26 November 2022 • Accepted 5 December 2022*)

Abstract−Photocatalytic degradation of dyes is one of the most effective methods that can be utilized for a pollution-free environment. For this purpose, Tungsten oxide (WO_3), zinc oxide (ZnO) and their composite WO_3/ZnO were synthesized using facile route. X-rays diffraction (XRD), Fourier transform infra-red spectroscopy (FTIR) and scanning electron microscopy (SEM) confirmed their structural, spectral and morphological features, respectively. These techniques confirmed the formation of desired products. The as-prepared samples were utilized as photocatalysts for the evaluation of the photocatalytic removal of methylene blue and rhodamine B under solar light irradiation. The obtained results showed that the synergistic effect of tungsten oxide and zinc oxide is responsible for the increased charge separation and reduction in recombination chances of charge carriers that enhance the remarkable photocatalytic performance. For methylene blue and rhodamine-b, the percentage degradation was 94% and 85.7%, respectively. Different scavenger studies showed that holes are the major active species responsible for the removal of methylene blue. The EIS and Mott-Schottky plots confirmed the p-type and n-type character of WO_3 and ZnO, respectively. Briefly, the as-synthesized nanocomposite showed enhanced photocatalytic behavior for the degradation of various dyes as compared to pristine metal oxides.

Keywords: Metal Oxide Nanoparticles, XRD, Photocatalysis, EIS, Mott-Schottky

INTRODUCTION

The increase in urbanization, global industrialization and population explosion has resulted in a decrease in the availability of healthy and pure water [1,2]. One of the main reasons behind this scarcity of drinkable water is the contamination of irremovable organic dyes that affect the water bodies tremendously [1,2]. Apart from these dyes, various other factors from commercial, agricultural and industrial areas are also responsible for creating toxic pollutants in water bodies. Scientists are striving to offer specific solutions to overcome these environmental problems [3]. Among these solutions, the best and cost-effective approach is the conversion of polluted water to healthy and fresh water. Solar light is free of cost and the most common element [4], which can be the best thing to degrade certain water pollutants using photocatalyst in a photocatalysis procedure. Semiconductor-based photocatalysis has gained great interest from scientists in environmental remediation because of its simplicity, low energy consumption and mild reaction conditions [7-10]. Metal oxide based photocatalysts have been extensively used for the degradation of various pollutants due to their abundance, greater life span, more light absorption, charge transport properties and electronic structure. These exceptional properties of metal oxides motivate us to choose them for the photocatalytic degradation of toxic dyes. ZnO is widely used as a raw material in the ceramic, cosmetic, glass and textile industries. It is an n-type semiconductor which has a band gap of 3.2 eV. The photocatalytic efficiency of ZnO has attained great interest as it has a great ability to degrade organic pollutants to H_2O and CO_2 [5,6]. The demerits of ZnO include its less efficiency and less stability due to photo-corrosion [7] as compared to TiO_2 (common photocatalyst).

To enhance its photocatalytic efficiency, two approaches can be made. The first one includes the changes in its properties, such as particle size and morphology [14-16]. The second approach involves improving the photocatalytic ability by metal ion doping [17-19], semiconductor coupling [6,8], noble metal deposition [9,10] or non-metal element doping [11]. Among these methods, an efficient way to improve the separation of photogenerated holes (h^+) and electrons (e^-) is semiconductor coupling, because the band gap of two different semiconductors would cause the separation of photo-produced e^- and h^+. WO_3 is a p-type semiconductor which has less energy gap of 2.7 eV and has conduction band and valence positions different from ZnO.

†To whom correspondence should be addressed.
E-mail: farooq.warsi@iub.edu.pk, mshakir@ucla.edu

For a pollution-free environment, the photocatalytic degradation of dyes is considered one of the most efficient, effective and cheap techniques. We have adopted this method owing to its unique benefits, such as cost-effectiveness, easy availability and formation of non-toxic products. For this, we have prepared WO_3, ZnO and WO_3/ZnO nanocomposite via facile and cost-effective wet precipitation method and ultrasonication method, respectively. These as-synthesized materials were characterized, and their photocatalytic and electrochemical measurements were studied to measure the degradation efficiency and flat band potential of as-synthesized material. Photocatalytic degradation using different types of scavengers was also examined to confirm which species is responsible for methylene blue degradation. This work will help to make new combinations of metal oxides nanocomposites having enhanced photocatalytic and electrochemical behavior.

EXPERIMENTAL SECTION

1. Chemicals

The following chemicals were utilized for synthesis of nanoparticles: $Zn(CH_3COO)_2{\cdot}2H_2O$, ($Na_2WO_4{\cdot}2H_2O$), Na_2CO_3 and concentrated HCl. The chemicals used during synthesis (obtained from Sigma Aldrich (Germany)) were of analytical grade and there was no need of further purification.

2. Synthesis of Nanoparticles of Zinc Oxide

The ZnO nanoparticles were fabricated by using sodium carbonate and zinc acetate dihydrate $(CH_3COO)_2Zn{\cdot}2H_2O$ by basic co-precipitation. 0.25 M and 0.5 M solutions of zinc acetate and sodium carbonate were prepared in distilled water separately. 30 ml of Na_2CO_3 solution was then added to zinc acetate solution gradually. The stirring was done continuously at 45 °C for 4 hours. The precipitates of $Zn(OH)_2$ were obtained having milky white appearance. The precipitates were then washed with distilled water until the pH became 7 and then dried in the oven. After drying, the precipitates were ground and calcination was done for 4 hours at 650 °C [12].

3. Synthesis of Nanoparticles of Tungsten Oxide

WO_3 nanoparticles were synthesized by the acid co-precipitation method. An aqueous solution of sodium tungstate dihydrate salt and concentrated HCl was used. In 0.1 M aqueous solution of sodium tungstate, 20 ml of HCl was added gradually. The stirring was done continuously for 2 hours. Yellowish precipitates of WO_3 were formed. Washing was done until the pH became neutral, then the precipitates were dried in an oven [13].

4. Synthesis of Nanocomposite (WO_3/ZnO)

The prepared samples were mixed in distilled water in an appropriate ratio and then ultra-sonicated for an hour. The obtained precipitates were placed in an oven for drying, and calcination was carried out at 650 °C for 4 hours. The synthesized nanocomposite (WO_3/ZnO) was confirmed by various characterization methods [14]. Fig. 1 clearly shows the schematic representation for the synthesis of metal oxides and their nanocomposite.

5. Characterization Techniques

The XRD patterns of the synthesized nano-oxide and their composite were obtained by utilizing Shimadzu 6100AS XRD instrument with the X-ray source Cu Kα (λ=0.15406 nm). The diffraction study was done at room temperature. FTIR analysis was conducted for the better determination of the structure and nature of the functional groups present in synthesized nano-oxides. The FTIR analysis was done with the help of the Shimadzu IRAffinity-1S spectrometer. For analysis of optical properties, Agilent Cary 60 spectrophotometer constituting spectral range of 200 nm-800 nm was utilized. For EIS analysis, Gamry interface 5000 within the frequency range of 10^2-10^6 Hz was used. In this analysis, 100 ml of 0.5 M NaCl solution was used for ZnO as an electrolyte, while 100 ml solution of 2 M H_2SO_4 was used for WO_3 and nanocomposite WO_3/ZnO as an electrolyte.

6. Photocatalytic Removal

The photocatalytic removal ability of WO_3, ZnO and WO_3/ZnO

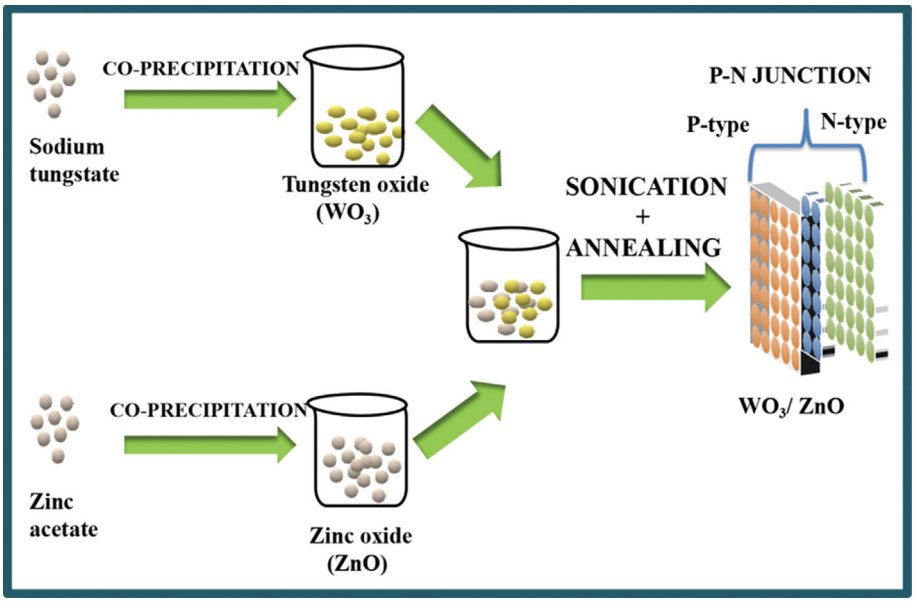

Fig. 1. Schematic diagram of synthesis of Metal oxide nanoparticles.

nanocomposite was noticed using MB and Rh-B as colorful contaminants. At first, 3 ppm solution of dye was prepared in 1 liter and used as a stock solution. 20 mg of the photocatalyst was added in a beaker containing 300 ml solution of dye. Then, the mixture was agitated with regular stirring, and whole apparatus was kept in the dark for about an hour for the study of the adsorption and desorption of photocatalyst on the dye's surface. After 1 hr, the sample mixture was transferred under solar radiation, and 3 ml off the sample was taken after regular intervals from the beaker. The absorption spectrum was obtained using UV-Vis spectrophotometer. The percentage removal of the photocatalyst was calculated by formula:

$$\% \text{ Degradation} = \left(1 - \frac{C_t}{C_0}\right) \times 100$$

where,

C_t=concentration of dye after irradiation

C_o=concentration of dye before irradiation.

RESULTS AND DISCUSSION

1. XRD

The numerous phases of the as-manufactured tungsten oxide (WO_3), zinc oxide and their nanocomposite (WO_3/ZnO) were determined and studied by using an X-ray diffractometer. For ZnO, from 20° to 80° range of 2$\theta$the diffraction peaks appeared at 29.9°, 35.5°, 37.8°, 48.6°, 60.1°, 63.5°, 67.5° and 77.7° as shown in Fig. 2(b). The Miller indices (100), (002), (101), (102), (103), (200), (112) and (202), respectively, compared with JCPDS card no. 00-001-1136 correlate with these diffraction peaks and indicates the synthesis of zinc metal nano-oxides. [15]. For WO_3, in range of 2θ=20° to 60° the diffraction patterns appeared at 25.9°, 34.7°, 43.2°, 46.2°, 49.4°, 52.6° and 56.7° as shown in Fig. 2(a). The Miller indices (120), (220), (221),(002), (012), (022) and (240), respectively, related to JCPDS card no. 01-075-2072 cor-relate with these diffraction patterns, which indicates the preparation of tungsten metal nano-oxides [16]. For nanocomposite, the diffraction peaks appeared at 25.7°, 34.7°, 43.2°, 46.3°, 49.5°, 52.7°, 56.6°, 61.9°, 64.8°, 69.5° and 78.3° as illustrated in Fig. 2(c). The Miller indices (120), (002), (221), (002), (012), (022), (240), (103), (200), (112) and (202), respectively, correlate with these peaks of diffraction, which indicate the preparation of tungsten metal nano-oxides as it has almost all the major peaks of metal nano-oxides. For determining the crystalline size of the as-synthesized metal nano-oxides and their nanocomposite, the Debye-Scherrer formula was used [17].

$$D = K\lambda\, \beta\cos\theta \quad (1)$$

In this formula, D shows crystalline size, K is Scherrer constant, λ is the X-ray wavelength for copper source which is equal to 1.5406 Å, FWHM is shown by β and θ represents Bragg's angle [18].

The preparation of WO_3 and ZnO crystals in the nanocomposite was restrained because the crystalline size of the pure metal nano-oxides was greater than the crystalline size of the nanocomposite. Two types of phases were identified in nanocomposite WO_3/ZnO from the X-ray diffraction pattern. Out of these phases, the orthorhombic phase represents WO_3 nanoparticles [19], while the hexagonal phase may represent the ZnO nanoparticles [20]. XRD patterns

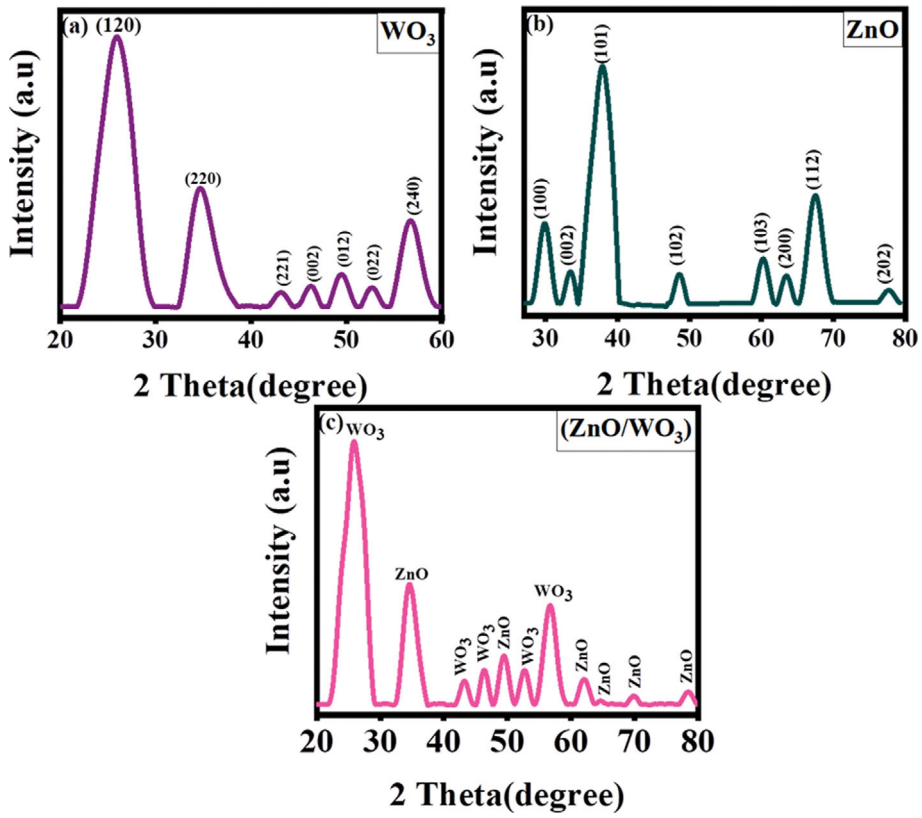

Fig. 2. XRD of WO_3, ZnO and their nanocomposite WO_3/ZnO, respectively.

Table 1. Parameters obtained from XRD of WO_3, ZnO and their nanocomposite WO_3/ZnO

Serial No.	Parameters	WO_3	ZnO
1)	Symmetry	Orthorhombic	Hexagonal
2)	Crystalline size D (nm)	2.4544	4.5118
3)	Lattice constant (a) Å	a=6.847	a=3.319
		b=7.417	c=5.236
		c=3.857	
4)	Cell volume V $(Å)^3$	195.87	57.678
5)	R-Square (R^2)	0.994	0.992
6)	Adj.R Square (R^2)	0.994	0.992

of the synthesized nanoparticles were utilized to calculate the percentage crystallinity of the particles by using the given formula:

Percentage Crystallinity
=(Area of Crystalline Peaks/Area of all peaks)×100

The percentage crystallinity of WO_3, ZnO and WO_3/ZnO calculated by using the above equation was 97.09%, 95.66% and 99.95%, respectively.

Different lattice parameters, including crystallite phases and size of metal nano-oxides and their nanocomposite, are recorded in Table 1.

2. Fourier Transform Infra-red Spectroscopy

The FTIR spectra of synthesized WO_3, ZnO and their nanocomposite WO_3/ZnO is shown in Fig. 3. Among the various techniques of infrared spectroscopy, FTIR spectroscopy has attained greater attention. FTIR spectra illustrate the analysis of various spectra of the synthesized nano-oxides and tell about the ions and bonds position in the crystal of as-synthesized oxides [21]. FTIR spectra were taken and analyzed between 4,000-400 cm^{-1}. In Fig. 3, the lowest peak (shown in purple color) illustrates the main absorption bands, which authenticate the formation of tungsten oxide. The peaks at approximately 851 cm^{-1} and 748 cm^{-1} are the main characteristic bands and show the stretching vibrations of the W-O functional group. Simultaneously, the absorption bands at around 3,469 cm^{-1} and 1,636 cm^{-1} illustrate the stretching vibration modes of the OH^- [22].

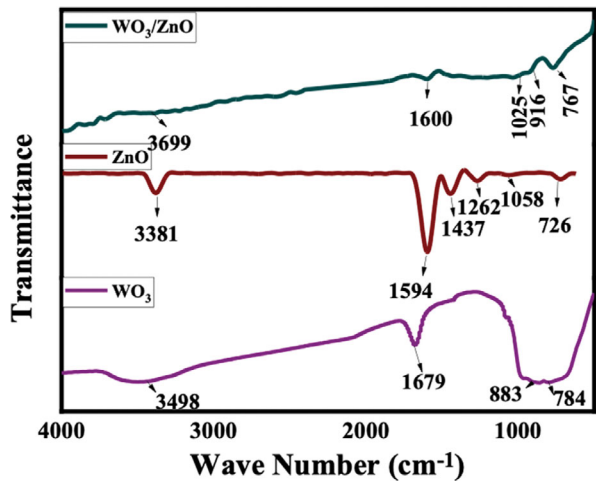

Fig. 3. FTIR Analysis of WO_3, ZnO and their nanocomposite WO_3/ZnO.

In Fig. 3, the middle curve (showed in red color) illustrates the stretching vibration modes of OH^- at 3,381 cm^{-1} and 1,594 cm^{-1}, 1,437 cm^{-1}. 1,262 cm^{-1} while the characteristic absorption bands at around 1,058 cm^{-1} and 726 cm^{-1} are accredited to the ZnO stretching vibration [23].

In Fig. 3, the highest peak (in green color) illustrates the stretching vibration modes at approximately 916 cm^{-1} (stretching vibrations of the W-O functional group) 767 cm^{-1} (ZnO), that elucidate the M-O-M bond stretch for the nanocomposite WO_3/ZnO (where M represents tungsten and zinc), while stretching vibrations at around 3,699 cm^{-1} and 1,600 cm^{-1} elucidate the hydroxyl group [35].

The stretching vibration modes for hydroxyl group, which may appear due to water molecule absorbed on the as-synthesized nano-oxides, perform a significant role in the process of photocatalysis. The reason is that the absorbed water molecules have the capability of providing various active sites for the stimulation of chemical reaction by reducing the photo-corrosion process of fabricated metal nano-oxides.

3. Optical Properties

The synthesized oxide nanoparticles and their nanocomposite have the potential to absorb the photons coming from sunlight irradiation on the basis of their band gap energies. The band gap analysis of the as-synthesized metal oxide nanoparticles (WO_3, ZnO) and the nanocomposite (WO_3/ZnO) was conducted by using the UV/Visible spectrophotometer and then the band gap energies for these samples were calculated by using a Tauc plot.

The Tauc plot equation is as [24].

$$(\alpha h\nu)^n = k(h\nu - E_g) \quad (2)$$

where, α is molar absorptive, h is Planck's constant, v is light frequency, A is light absorbance by photocatalyst, E_g is band gap energy and n is the different values based on transition type [25]. The UV/Visible spectra and the Tauc plots of WO_3, ZnO and their nanocomposite WO_3/ZnO are demonstrated in Figs. 4 and 5; the direct band gap energies of the prepared samples are illustrated in Table 2. The prepared nanocomposite WO_3/ZnO has lesser band-gap energy than that of pure oxide nanoparticles, making the nanocomposite more effective for various dyes by photo-degradation under solar light illumination. Due to the increase in band gap energy, the absorption of photons decreases in the visible light spectrum. It also induces more chances of recombination of photogene-

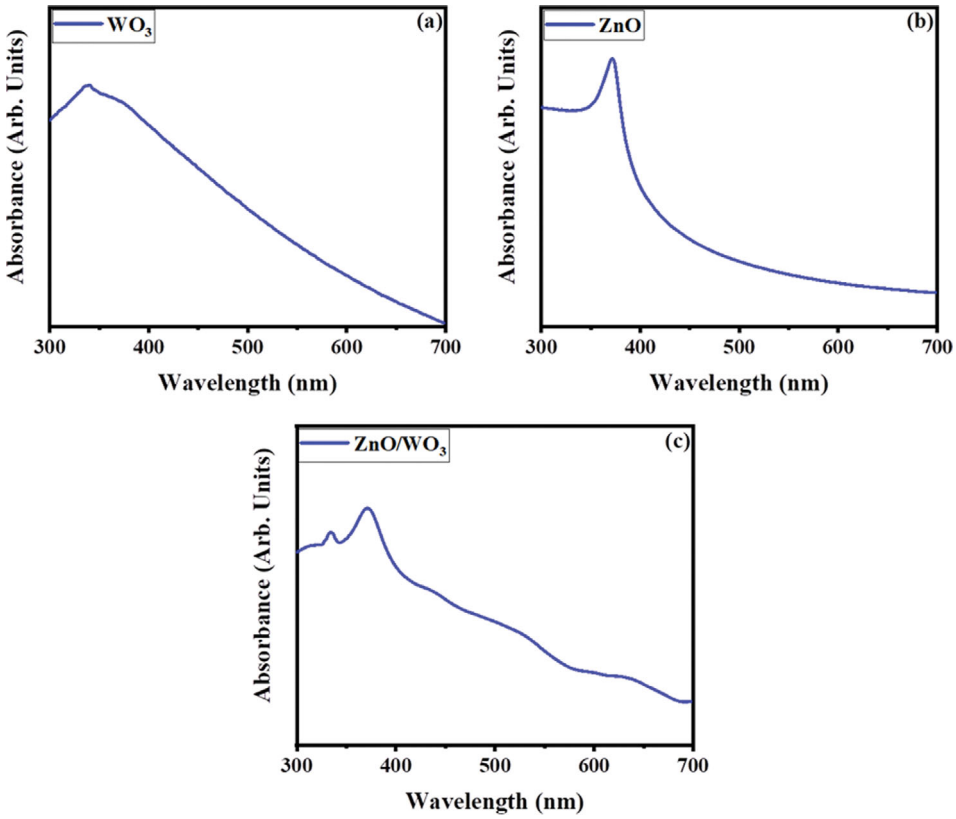

Fig. 4. UV-Visible spectra of WO_3, ZnO and their nanocomposite WO_3/ZnO.

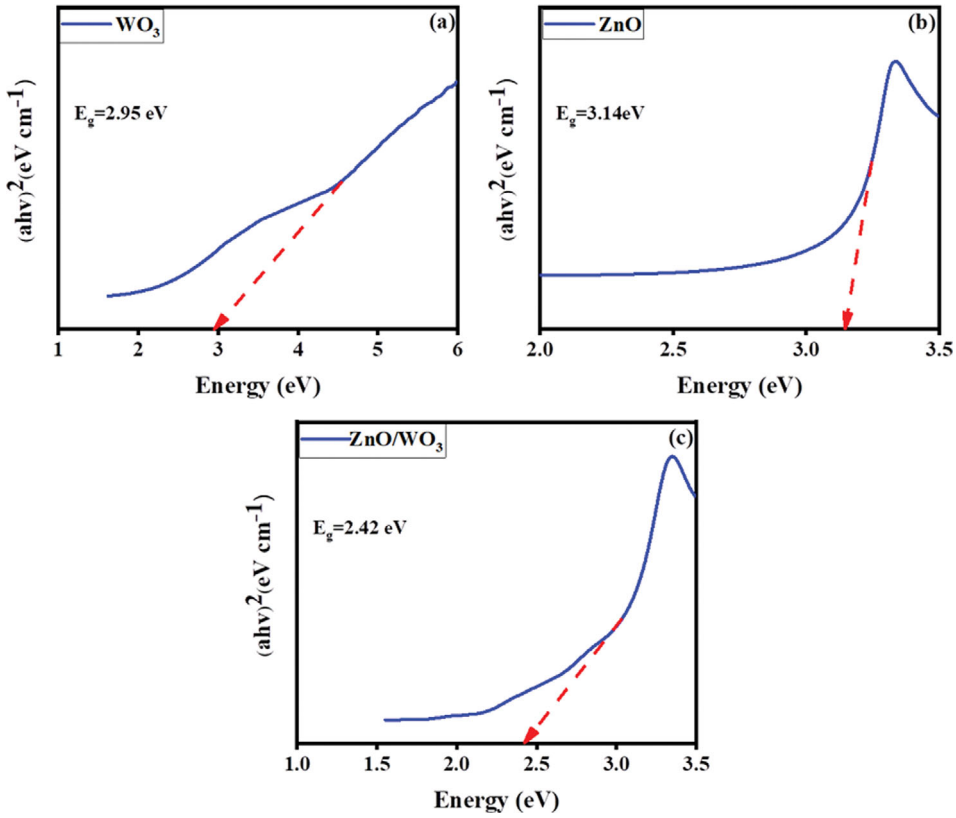

Fig. 5. Tauc plots of WO_3, ZnO and their nanocomposite WO_3/ZnO.

Table 2. Direct band-gap values of WO_3, ZnO and their nanocomposite WO_3/ZnO

Serial No.	Name	Band gap (eV)
1.	WO_3	2.95
2.	ZnO	3.14
3.	WO_3/ZnO	2.42

rated species like electrons and holes due to which photocatalytic degradation ability of catalyst is reduced [26].

4. SEM Analysis

The morphological analysis of the as-synthesized samples was confirmed using SEM analysis. Fig. 6(a) shows the SEM analysis of WO_3, which is spherical in shape and the particle size calculated for them is 279.8 nm. Fig. 6(b) shows the granular morphology of ZnO and the particle size calculated for zinc oxide nanoparticles is 261.5 nm. While the complex morphology of nanocomposite WO_3/ZnO showed the presence of both WO_3 and ZnO.

5. Photocatalysis

The photocatalytic removal of rhodamine b (Rh-B) and methylene blue (MB) was analyzed using WO_3, ZnO and WO_3/ZnO nanocomposite as photocatalyst. Fig. 7 illustrates the photolysis test of methylene blue. In this test, it can be clearly seen that methylene blue can be degraded to some extent in the presence of sunlight without any addition of photocatalyst. Fig. 8 shows the absorption spectra of MB dye taken after regular time intervals to study the degradation efficiency of as-synthesized nanomaterials under solar radiation. The removal ability of pure metal oxides is lower than the nanocomposite due to electron-hole pair recombination and higher band gap energy of metal oxides [27]. The main reason behind the increase in degradation ability of WO_3/ZnO nanocomposite was attributed to fewer recombination chances of e^--h^+ pair

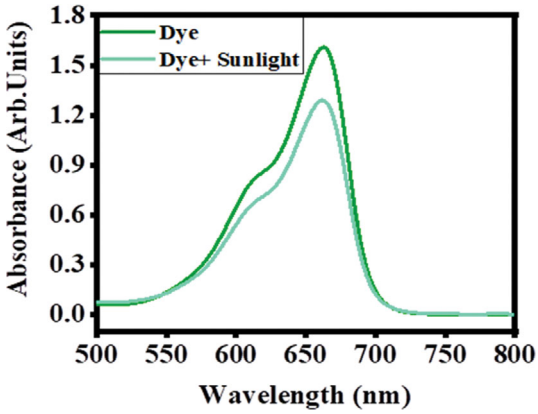

Fig. 7. Photolysis test of Methylene Blue (MB).

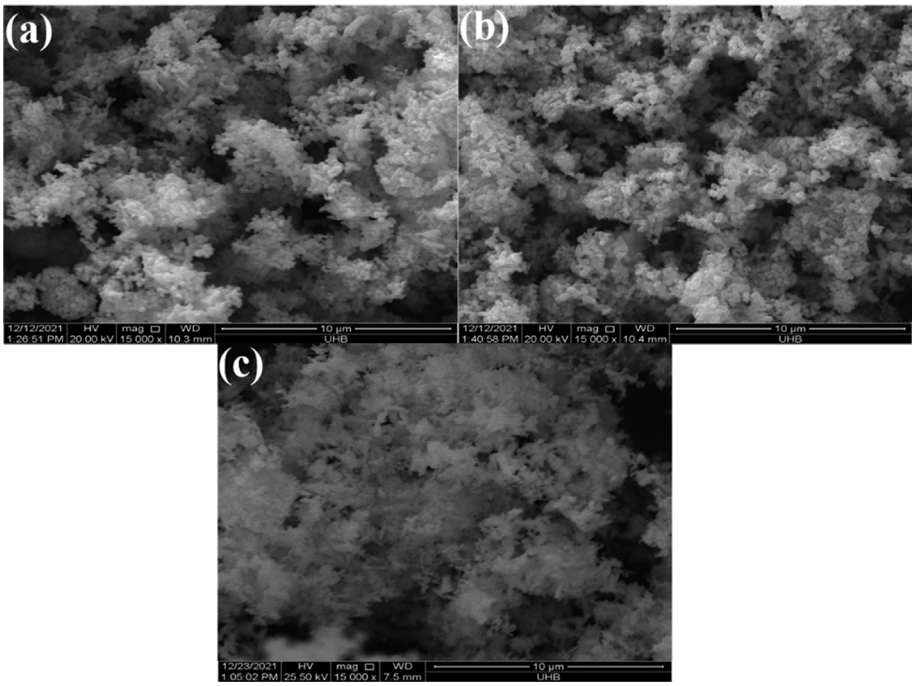

Fig. 6. SEM images of (a) WO_3, (b) ZnO and (c) their nanocomposite WO_3/ZnO.

Table 3. Comparison of percentage removal of MB and Rh-B with WO_3, ZnO and their nanocomposite WO_3/ZnO

Serial No.	Photocatalyst	Percentage removal of MB	Percentage removal of Rh-B
1.	WO_3	79.6%	66%
2.	ZnO	91.6%	78%
3.	WO_3/ZnO	94%	85.7%

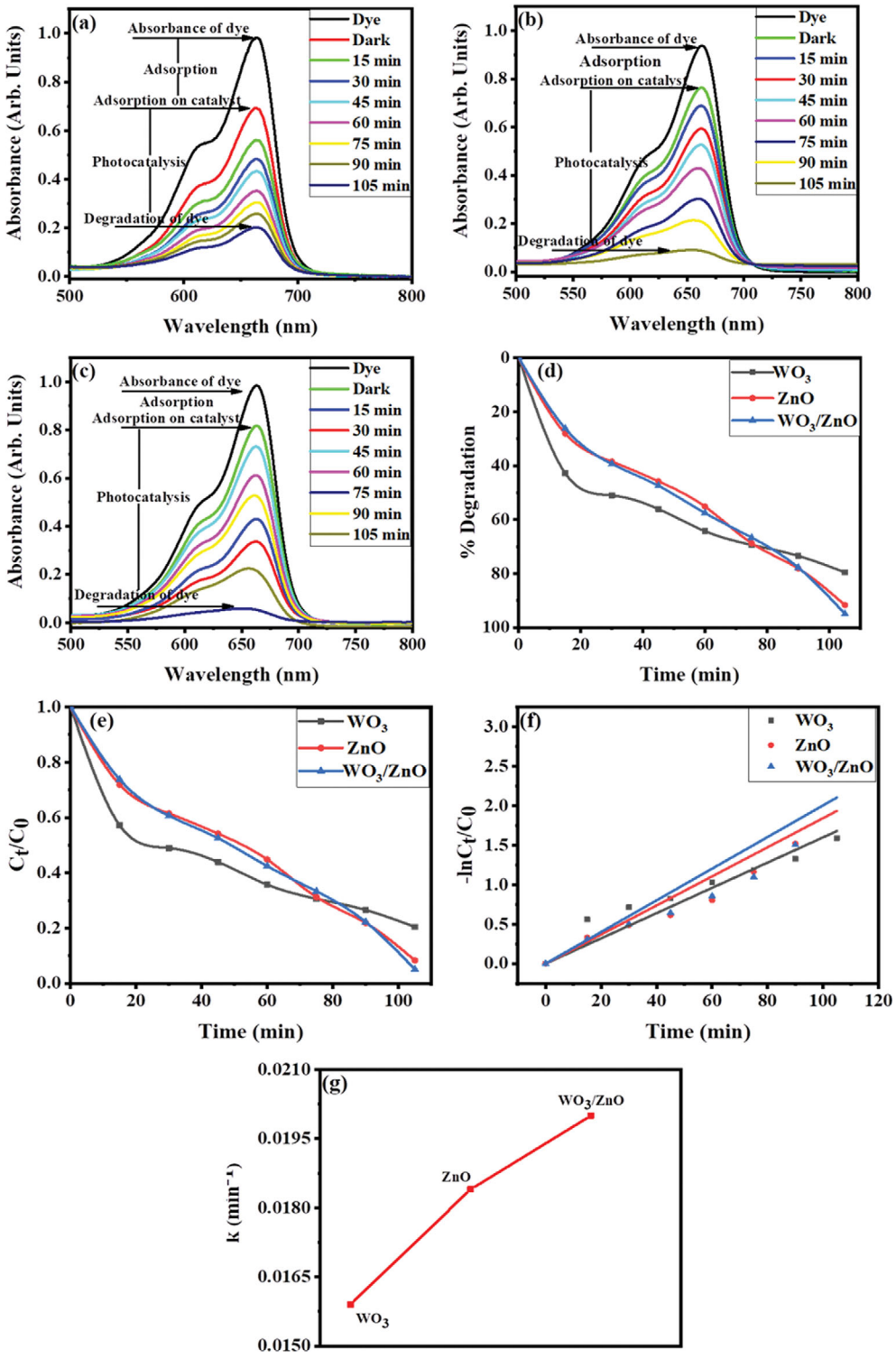

Fig. 8. Removal spectra of MB with WO_3, ZnO and their nanocomposite WO_3/ZnO.

and lower optical band gap energy.

Table 3 shows the comparison between percentage degradation of pure metal oxides and their nanocomposite. It is proved that WO_3/ZnO nanocomposite showed greater degradation efficiency, which is 94% and 85.7% for MB and Rh-B, respectively, than pure metal oxides. A kinetic study was also done to explore the photocatalytic reaction in detail. For this purpose, the kinetic equation for the pseudo first-order reaction was applied [28].

$$\ln\frac{Ao}{At} = Kt$$

The results calculated from the above equation can be seen in

Table 4. Comparison of rate constants for MB and Rh-B degradation with WO_3, ZnO and their nanocomposite WO_3/ZnO, respectively, with different scavengers

Serial No.	Photocatalyst	Reaction rate constant (min^{-1}) WO_3	Reaction rate constant (min^{-1}) ZnO	Reaction rate constant (min^{-1}) WO_3/ZnO
	MB	0.0159	0.0184	0.02
	Rh-B	0.008	0.0122	0.0125
	MB+Isopropyl Alcohol	0.012	0.026	0.028
	MB+EDTA	0.015	0.016	0.018
	MB+vitamin C (ascorbic acid)	0.016	0.02	0.027
	MB+$AgNO_3$	0.017	0.0195	0.02

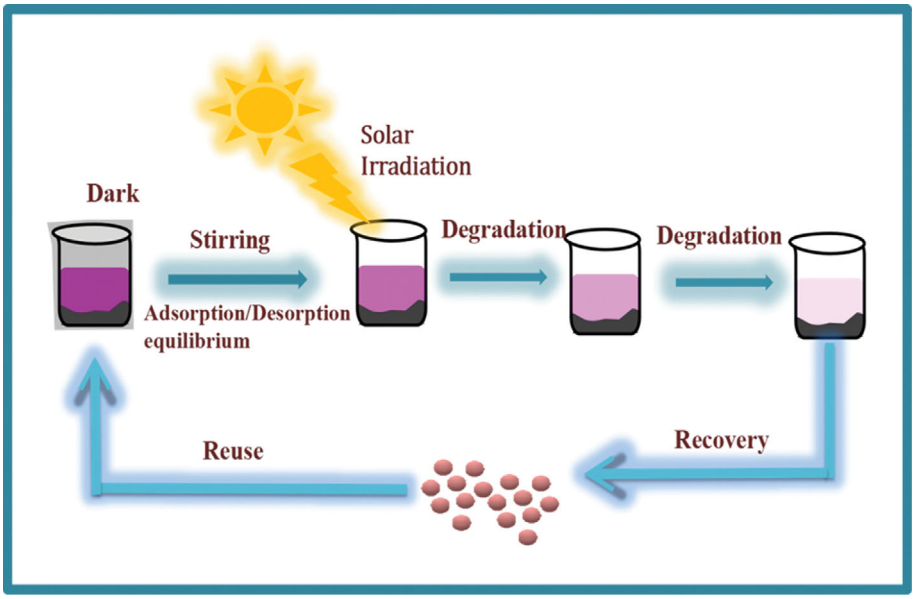

Fig. 9. Schematic diagram showing the photocatalysis process.

Table 4, which shows the rate constant of photocatalytic degradation reaction using WO_3, ZnO and WO_3/ZnO nanocomposite. The general schematic diagram for the process of photocatalysis can be seen in Fig. 9 that gives the main idea how photocatalytic degradation of dyes proceeds.

5-1. Role of Scavenger and Mechanism of Photocatalysis

Scavenger studies were performed to study the reactive species responsible for the removal under solar radiation. Ethylenediaminetetraacetic acid (EDTA) was utilized as scavenger of holes. Silver nitrate ($AgNO_3$) was used as a quencher of electrons. In the same way, ascorbic acid and Isopropyl alcohol were utilized for quenching ($*O2^{-2}$) superoxide anion radicals and (*OH) hydroxyl radicals [6,7]. Fig. 10 shows the degradation variation of methylene blue by as-synthesized photocatalyst using EDTA scavengers.

Fig. 10, S2, S3 and S4 shows the results of this quenching experiment, and it was found from Fig. 10 that holes are the major reactive species responsible for the degradation of methylene blue.

Based on these scavenger studies, the proposed procedure of photocatalytic removal of dye as shown in Fig. 11 is as follows:

1. $WO_3/ZnO+hv \rightarrow hvWO_3/ZnO\ (e^-_{CB}+h^+_{VB})$

2. $WO_3/ZnO\ (e^-)+O^2 \rightarrow \cdot O_2^-$

3. $WO_3/ZnO\ (h^+)+OH^- \rightarrow \cdot OH+WO_3/ZnO$

4. $\cdot O_2^- + H_2O \rightarrow \cdot OOH+OH^- \rightarrow H_2O_2$

5. $H_2O_2+{}^{\cdot}O_2^- \rightarrow {}^{\cdot}OH+OH^-$

6. $Dye+\cdot OH+\cdot O_2 \rightarrow$ Degradation products

The first step involves the adsorption of dye molecules on the surface of synthesized photocatalyst. Dye sensitization of ZnO in WO_3/ZnO nanocomposite takes place because of this adsorption. Due to solar light, the excitation of electrons (e^-) takes place from VB (valence band) to the CB (conduction band) of dye-sensitized ZnO and WO_3, and the same amount of holes (h^+) are produced in VB as mentioned in Eq. (1). The WO_3 has more negative VB potential than ZnO, which has more positive CB potential. So, the photogenerated electrons (e^-) were moved from WO_3 to ZnO's surface across the WO_3/ZnO nanocomposite interface. In the meantime, photogenerated holes were moved from ZnO toWO_3. The active free radical species ($^{\cdot}OH$, O^{2-}) will result from the reaction between dissolved oxygen (O_2) (Eqs. (2)-(5)). It was proved from

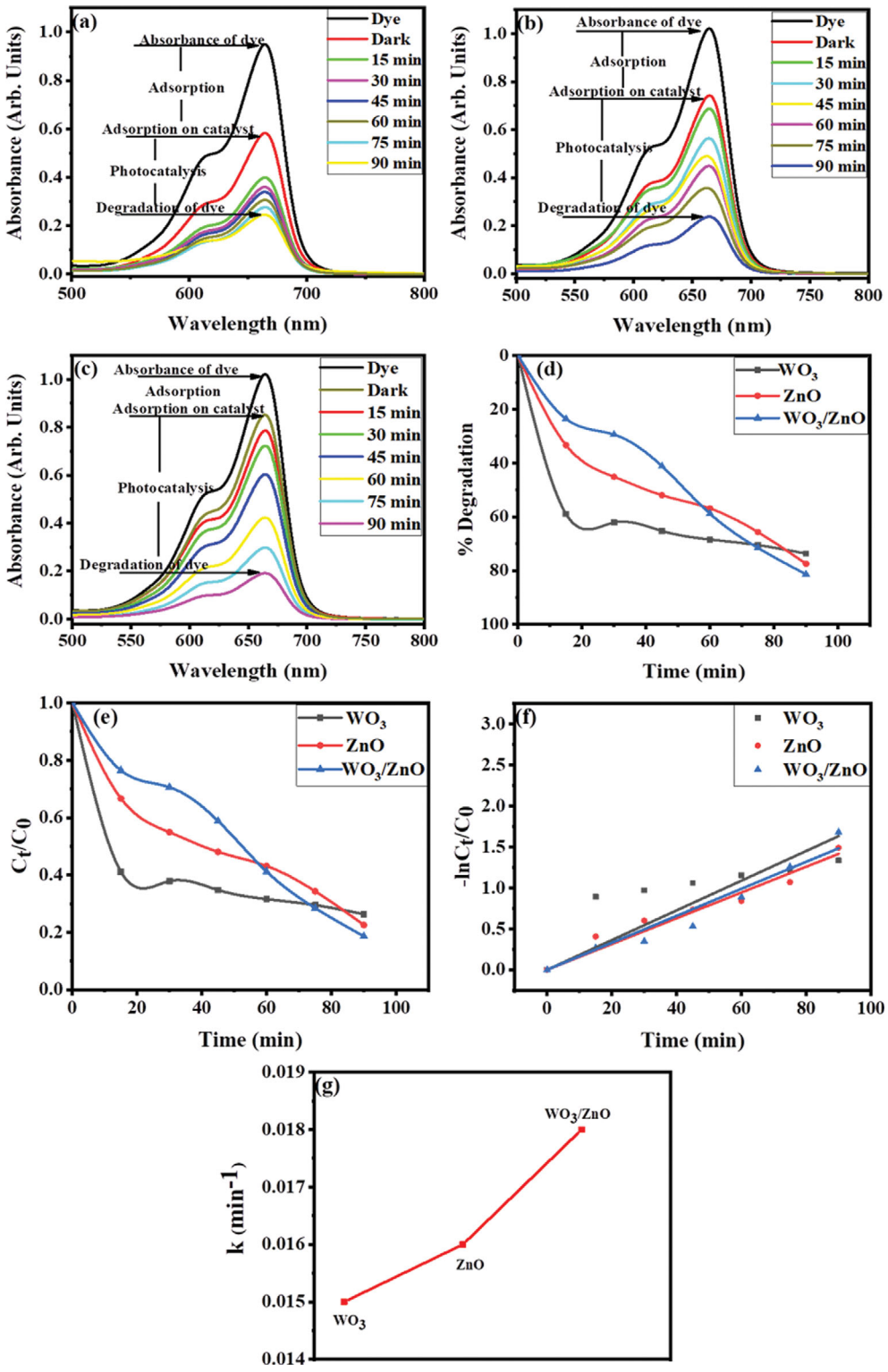

Fig. 10. Removal spectra of MB with WO_3, ZnO and their nanocomposite WO_3/ZnO using EDTA as scavenger.

the data given in Table 5 that these holes are the main species in charge of the removal and ring-opening reaction of dye molecules. It can be seen from Fig. 12 and Fig. 13 that these metal oxides and their nanocomposite can be recycled and reused again and again even after many cycles. The comparative study of our current work with already reported literature can be seen in Table 6, which demonstrates the percentage degradation of different dyes using different metal oxides under various light sources. Methylene blue showed greater photocatalytic efficiency than Rhodamine B with as-synthesized photocatalysts because it depends upon the interaction of

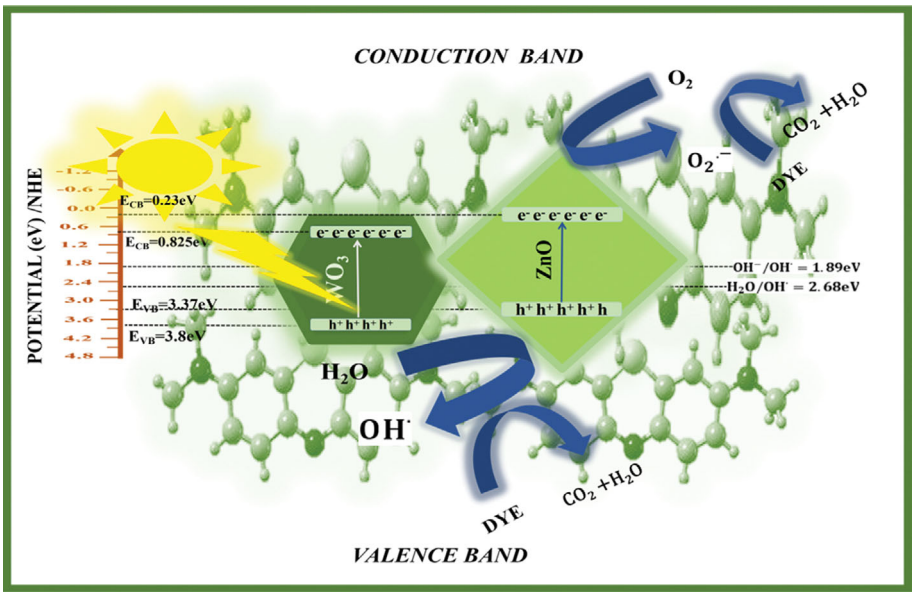

Fig. 11. Schematic diagram of photocatalytic removal of various dyes by WO_3, ZnO and their nanocomposite WO_3/ZnO as a photocatalyst.

Table 5. Comparison of percentage removal of MB with WO_3, ZnO and their nanocomposite WO_3/ZnO, respectively, with different scavengers

S.N.	Photocatalyst	Isopropyl alcohol	Ethylenediamine tetra-acetic acid (EDTA)	Vitamin C	$AgNO_3$
1.	WO_3	62.8%	73.6%	83.9%	80%
2.	ZnO	84.6%	77.4%	89.6%	87.6%
3.	WO_3/ZnO	88.4%	81.35%	97.5%	91.3%

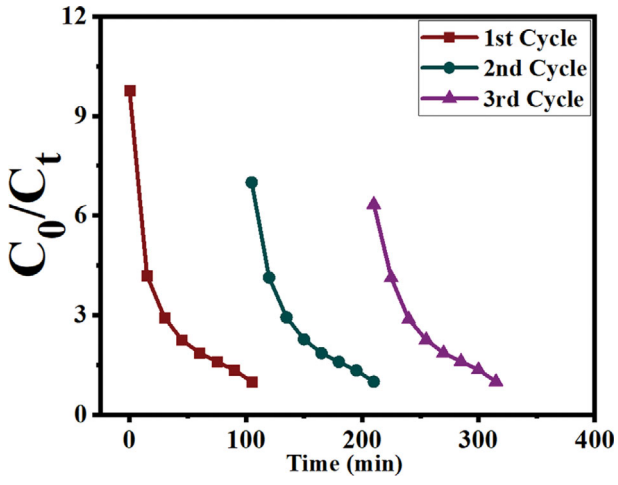

Fig. 12. Recyclability of as-synthesized samples after three cycles.

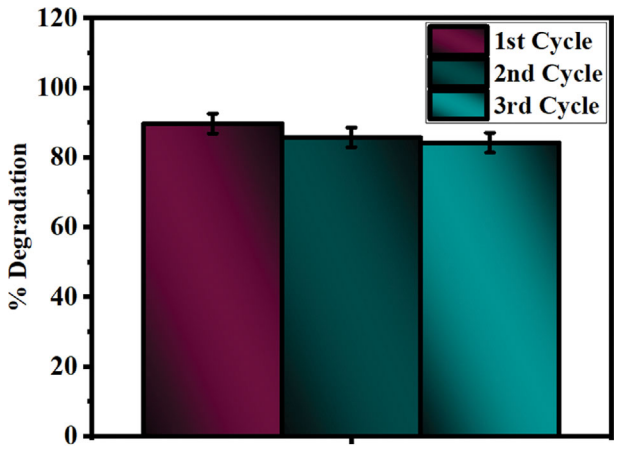

Fig. 13. Reusability of as-synthesized samples after three cycles having error bars.

photocatalyst and dye. The degradation of a particular dye varies with the semiconductor used in the reaction. It also depends on many other factors like activity of reactive intermediates, solution pH, adsorption of dye on the photocatalyst surface etc.

Fig. 14 shows a bar chart of the comparison between percentage degradation of MB and Rh-B, while the comparison between percentage degradation of methylene blue dye using as-synthesized nanoparticles and their nanocomposite with different scavengers can be seen clearly in Fig. 15. It was noticed that EDTA showed lowest degradation efficiency, that confirmed that holes are the main species responsible for the degradation of dye.

6. Electrochemical Impedance Spectroscopy

Electrochemical impedance spectroscopy (EIS) was used under frequency ranging from 10^2 Hz to 10^6 Hz in 100 ml of 0.1 M NaCl

Table 6. Comparison table of current work with the reported literature

Sr. No.	Photocatalyst	Contaminant	Radiation source	Percentage degradation	Reference
1.	ZnO/Ag	MO	Visible light	78%	[29]
2.	NiO/Ag	MO	Visible light	42%	[29]
3.	AgO	MO	Visible light	60.5%	[30]
5.	SnO_2	Congo red	Solar radiation	90%	[31]
6.	CdO	Alizarin red S	Solar radiation	78%	[32]
7.	ZrO_2	MB	UV-light	99%	[33]
8.	NiO	Evans blue	Solar radiation	88.13%	[34]
9.	WO_3	MB	Solar radiation	79.6%	Present Work
10.	ZnO	MB	Solar radiation	91.6%	Present Work
11.	WO_3/ZnO	MB	Solar radiation	94%	Present Work
12.	WO_3	Rh-B	Solar radiation	66%	Present Work
13.	ZnO	Rh-B	Solar radiation	78%	Present Work
14.	WO_3/ZnO	Rh-B	Solar radiation	85.7%	Present Work

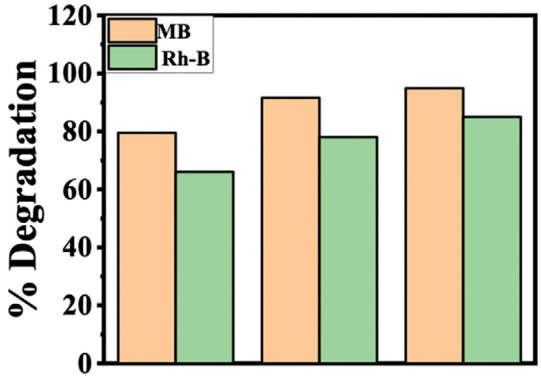

Fig. 14. Percentage of photocatalytic degradation of methylene blue and Rhodamine-B.

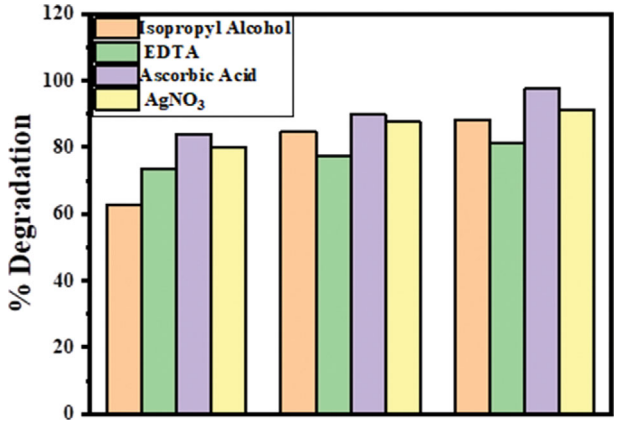

Fig. 15. Comparison of percentage degradation of Methylene blue and Rhodamine-B with WO_3, ZnO and their nanocomposite WO_3/ZnO, respectively, with various scavengers.

and 0.2 M H_2SO_4 electrolyte for ZnO and WO_3, respectively. Reference electrode and counter electrode of Silver-silver chloride Ag(s)/AgCl(s) and platinum wire were utilized, respectively. 5 mg of as-prepared sample was mixed with Nafion to made slurry, which

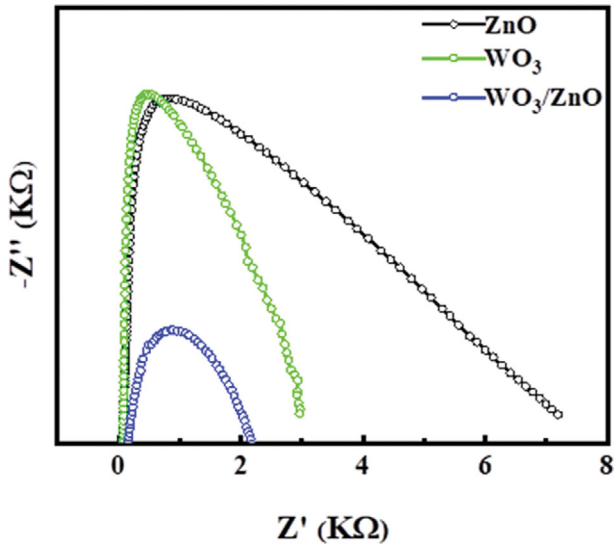

Fig. 16. EIS of WO_3, ZnO and their nanocomposite WO_3/ZnO.

was used in preparation of working electrode. A thin coating of this slurry was applied on Indium-Tin oxide (ITO) coated glass. In the very next step, the prepared working electrode was dried at room temperature for 1 hr. The charge transfer properties of as-prepared samples were determined by EIS. In Fig. 16, it can be seen clearly that diameter of Nyquists's semicircle of WO_3/ZnO nanocomposite is smaller as compared to pure WO_3 and ZnO nano-oxides [28,35].

The main reason behind this smaller diameter is lesser charge transfer resistance which helps in the separation of photo-generated electron-hole pair, also transfer charges between interfaces and also decreases the possibility of recombination of electron/holes.

The Mott-Schottky plot was also drawn as in Fig. 17, which confirms the p-type character (ascending peak) of WO_3 n-type character (descending peak) of ZnO. The flat band potential of as-prepared metal oxides was also measured by this plot, and the values of flat band potential for WO_3 and ZnO are illustrated in Table 7.

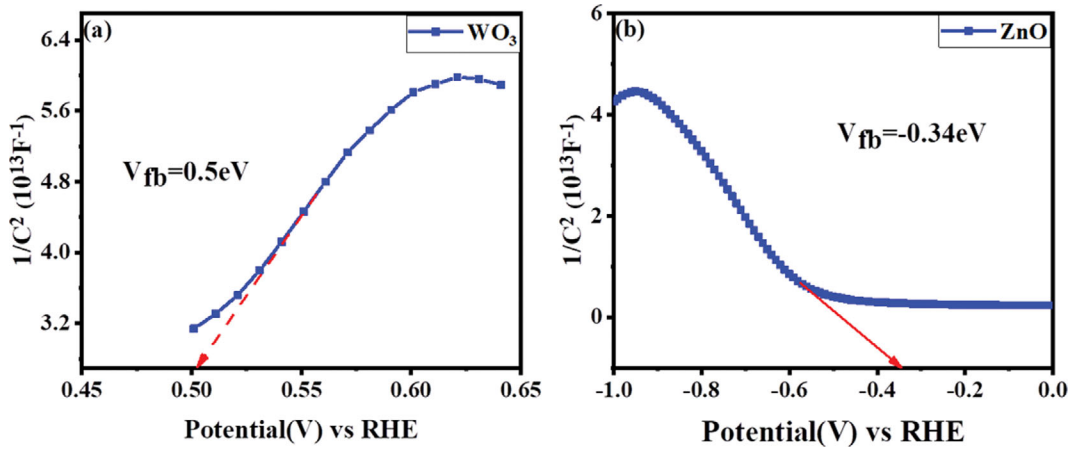

Fig. 17. Mott-Schottky plots of WO_3, ZnO and their nanocomposite WO_3/ZnO respectively.

Table 7. Flat band potential of WO_3 and ZnO oxides

Serial No.	Name	Flat band (eV)
	WO_3	0.5
	ZnO	−0.34

CONCLUSION

WO_3, ZnO andWO_3/ZnO nanocomposite, successfully synthesized using co-precipitation and ultra-sonication route, respectively, behaved as an effective photocatalyst for the removal of rhodamine b (Rh-B) and methylene blue (MB) under solar light exposure. The metal-oxygen-metal interaction in the nanocomposite is responsible for improved chemical reactivity, physical and structural properties. The nanocomposite showed 85.7% and 94% degradation within 120 min and 105 min with rhodamine-b and methylene blue, respectively, which is far better than pure metal oxides. Scavenger studies proved that holes are the main reason behind this extraordinary photocatalytic degradation ability. The Mott-Schottky plot confirms the p-type and n-type character of WO_3 and ZnO, respectively. The value of flat band potential calculated from Mott-Schottky plot is 0.5 eV for WO_3 and −0.34 eV for ZnO. The exceptional rate of degradation of WO_3/ZnO nanocomposite opens new doors for the synthesis of more such combinations having new characteristics in order to remove organic and toxic compounds from water.

ACKNOWLEDGEMENTS

Authors sincerely appreciate the King Khalid University for the research grant (KKU/RCAMS/22) under the Research Center for Advanced Materials Science (RCAMS) at King Khalid University, Saudi Arabia. Authors are also thankful to the Institute of Chemistry, Baghdad-ul-Jadeed Campus, The Islamia University of Bahawalpur and Higher Education Commission (HEC) Islamabad, Pakistan.

CONFLICT OF INTEREST

Authors declare no conflict of interest for this article.

SUPPORTING INFORMATION

Additional information as noted in the text. This information is available via the Internet at http://www.springer.com/chemistry/journal/11814.

REFERENCES

1. M. A. Tofighy and T. Mohammadi, *Desalination*, **258**, 182 (2010).
2. H. Daraei, A. Maleki, A. H. Mahvi, Y. Zandsalimi, L. Alaei and F. Gharibi, *Desalination and Water Treatment*, **52**, 6745 (2014).
3. W.-Q. Lu, S.-H. Xie, W.-S. Zhou, S.-H. Zhang and A.-L. Liu, *Open Environ. Sci. J.*, **2**, 1 (2008).
4. D. Pimentel, B. Berger, D. Filiberto, M. Newton, B. Wolfe, E. Karabinakis, S. Clark, E. Poon, E. Abbett and S. Nandagopal, *BioScience*, **54**, 909 (2004).
5. D. Chu, Y. Masuda, T. Ohji and K. Kato, *Langmuir*, **26**, 2811 (2010).
6. Y. Changlin, Y. Kai, S. Qing, C. Y. Jimmy, C. Fangfang and L. Xin, *Chin. J. Catal.*, **32**, 555 (2011).
7. L. Mingce and C. Weimin, *Chin. J. Catal.*, **29**, 881 (2008).
8. C. Wang, X. Wang, B.-Q. Xu, J. Zhao, B. Mai, G. Sheng and J. Fu, *J. Photochem. Photobiol. A: Chem.*, **168**, 47 (2004).
9. M. A. Bhatti, K. F. Almaani, A. A. Shah, A. Tahira, A. D. Chandio, A. Q. Mugheri, A. liaquat Bhatti, B. Waryani, S. S. Medany and A. Nafady, *J. Cluster Sci.*, **33**, 1445 (2022).
10. J. Xu, Y. Chang, Y. Zhang, S. Ma, Y. Qu and C. Xu, *Appl. Surf. Sci.*, **255**, 1996 (2008).
11. L.-C. Chen, Y.-J. Tu, Y.-S. Wang, R.-S. Kan and C.-M. Huang, *J. Photochem. Photobiol. A: Chem.*, **199**, 170 (2008).
12. K. Raja, P. Ramesh and D. Geetha, *Spectroc. Acta Pt. A-Molec. Biomolec. Spectr.*, **120**, 19 (2014).
13. H. I. Nogueira, A. M. Cavaleiro, J. Rocha, T. Trindade and J. D. P. de Jesus, *Mater. Res. Bull.*, **39**, 683 (2004).
14. S. Yousaf, T. Kousar, M. B. Taj, P. O. Agboola, I. Shakir and M. F. Warsi, *Ceram. Int.*, **45**, 17806 (2019).
15. S. Muthukumaran and R. Gopalakrishnan, *Opt. Mater.*, **34**, 1946 (2012).
16. R. Fatima, M. F. Warsi, M. I. Sarwar, I. Shakir, P. O. Agboola, M. F. A. Aboud and S. Zulfiqar, *Ceram. Int.*, **47**, 7642 (2021).

17. M. Aadil, S. Zulfiqar, H. Sabeeh, M. F. Warsi, M. Shahid, I. A. Alsafari and I. Shakir, *Ceram. Int.*, **46**, 17836 (2020).
18. A. Patterson, *Phys. Rev.*, **56**, 978 (1939).
19. E. Salje, *Acta Crystallogr. Sect. B: Struct. Crystallogr. Cryst. Chem.*, **33**, 574 (1977).
20. Y. Chen, R. Yu, Q. Shi, J. Qin and F. Zheng, *Mater. Lett.*, **61**, 4438 (2007).
21. M. A. Khan, M. Sabir, A. Mahmood, M. Asghar, K. Mahmood, M. A. Khan, I. Ahmad, M. Sher and M. F. Warsi, *J. Magn. Magn. Mater.*, **360**, 188 (2014).
22. N. Hiroshiba, Y. Tabata, S. Yamauchi and Y. Ichikawa, *Trans. Mater. Res. Soc. Jpn.*, **39**, 423 (2014).
23. G. Nagaraju, S. Prashanth, M. Shastri, K. Yathish, C. Anupama and D. Rangappa, *Mater. Res. Bull.*, **94**, 54 (2017).
24. A. Rahman, M. Aadil, M. Akhtar, M. F. Warsi, A. Jamil, I. Shakir and M. Shahid, *Ceram. Int.*, **46**, 13517 (2020).
25. R. Estrada, N. Djohan, D. Pasole, M. Dahrul, A. Kurniawan, J. Iskandar and H. Hardhienata, *The optical band gap of $LiTaO_3$ and Nb_2O_5-doped $LiTaO_3$ thin films based on Tauc Plot method to be applied on satellite*, IOP Conference Series: Earth and Environmental Science, IOP Publishing, 012092 (2017).
26. W. Zheng, Y. Chen, X. Peng, K. Zhong, Y. Lin and Z. Huang, *Materials*, **11**, 1253 (2018).
27. R. F. de Mello Peters, P. A. M. dos Santos, T. C. Machado, D. A. R. Lopez, Ê. L. Machado and A. d. A. L. Rodriguez, *Eclética Química*, **43**, 26 (2018).
28. E. Pehlivan, G. A. Niklasson, C. G. Granqvist and P. Georén, *Phys. Status Solidi (a)*, **207**, 1772 (2010).
29. H. Karimi-Maleh, B. G. Kumar, S. Rajendran, J. Qin, S. Vadivel, D. Durgalakshmi, F. Gracia, M. Soto-Moscoso, Y. Orooji and F. Karimi, *J. Mol. Liq.*, **314**, 113588 (2020).
30. J. Zhang, E. Ding, S. Xu, Z. Li, A. Fakhri and V. K. Gupta, *Int. J. Biol. Macromol.*, **164**, 1584 (2020).
31. K. Karthik, V. Revathi and T. Tatarchuk, *Mol. Cryst. Liq. Cryst.*, **671**, 17 (2018).
32. V. Revathi and K. Karthik, *Chem. Data Collections*, **21**, 100229 (2019).
33. K. Karthik, M. Madhukara Naik, M. Shashank, M. Vinuth and V. Revathi, *J. Cluster Sci.*, **30**, 311 (2019).
34. K. Karthik, M. Shashank, V. Revathi and T. Tatarchuk, *Mol. Cryst. Liq. Cryst.*, **673**, 70 (2018).
35. A. Bohe, J. Vilche, K. Jüttner, W. Lorenz and W. Paatsch, *Electrochim. Acta*, **34**, 1443 (1989).

Supporting Information

Zinc oxide-tungsten oxide (ZnO-WO_3) composite for solar light-assisted degradation of organic dyes

Fatima Aziz[*], Al-Zoha Warsi[*], Hamoud H. Somaily[,***], Muhammad Imran Din[****], Humera Sabeeh[*], Muhammad Farooq Warsi[*,†], and Imran Shakir[*****,†]**

*Institute of Chemistry, Baghdad-ul-Jadeed Campus, The Islamia University of Bahawalpur, Bahawalpur 63100, Pakistan
**Research Center for Advanced Materials Science (RCAMS), King Khalid University, Abha 61413, P.O. Box 9004, Saudi Arabia
***Department of Physics, Faculty of Science, King Khalid University, P.O. Box 9004, Abha, Saudi Arabia
****School of Chemistry, University of the Punjab, New Campus, Lahore 54590, Pakistan
*****Department of Materials Science and Engineering, University of California, Lose Angles, United States of America
(*Received 11 August 2022 • Revised 26 November 2022 • Accepted 5 December 2022*)

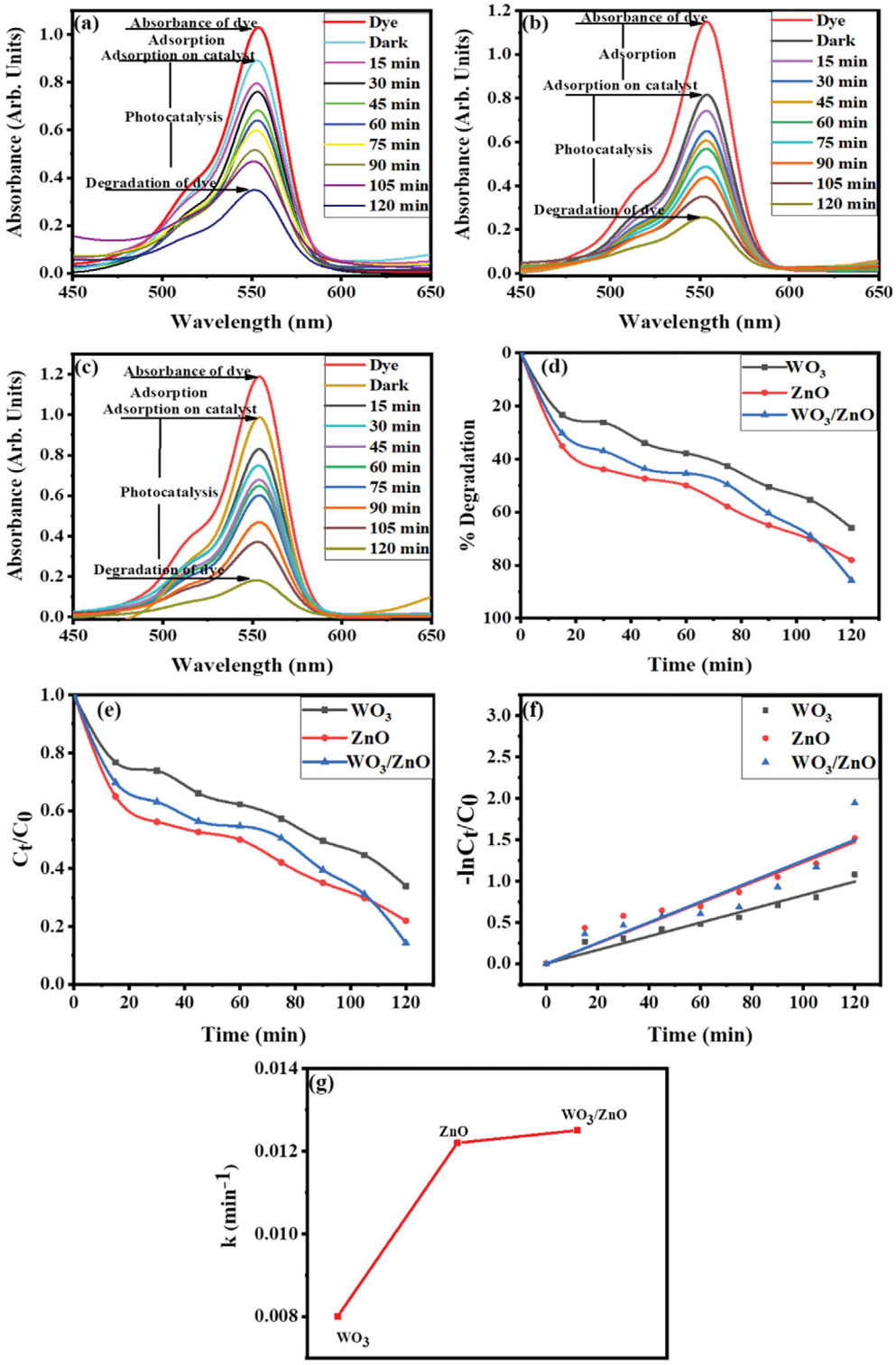

Fig. S1. Degradation spectra of rhodamine-b with WO_3, ZnO and their hetero-metallic oxide WO_3/ZnO.

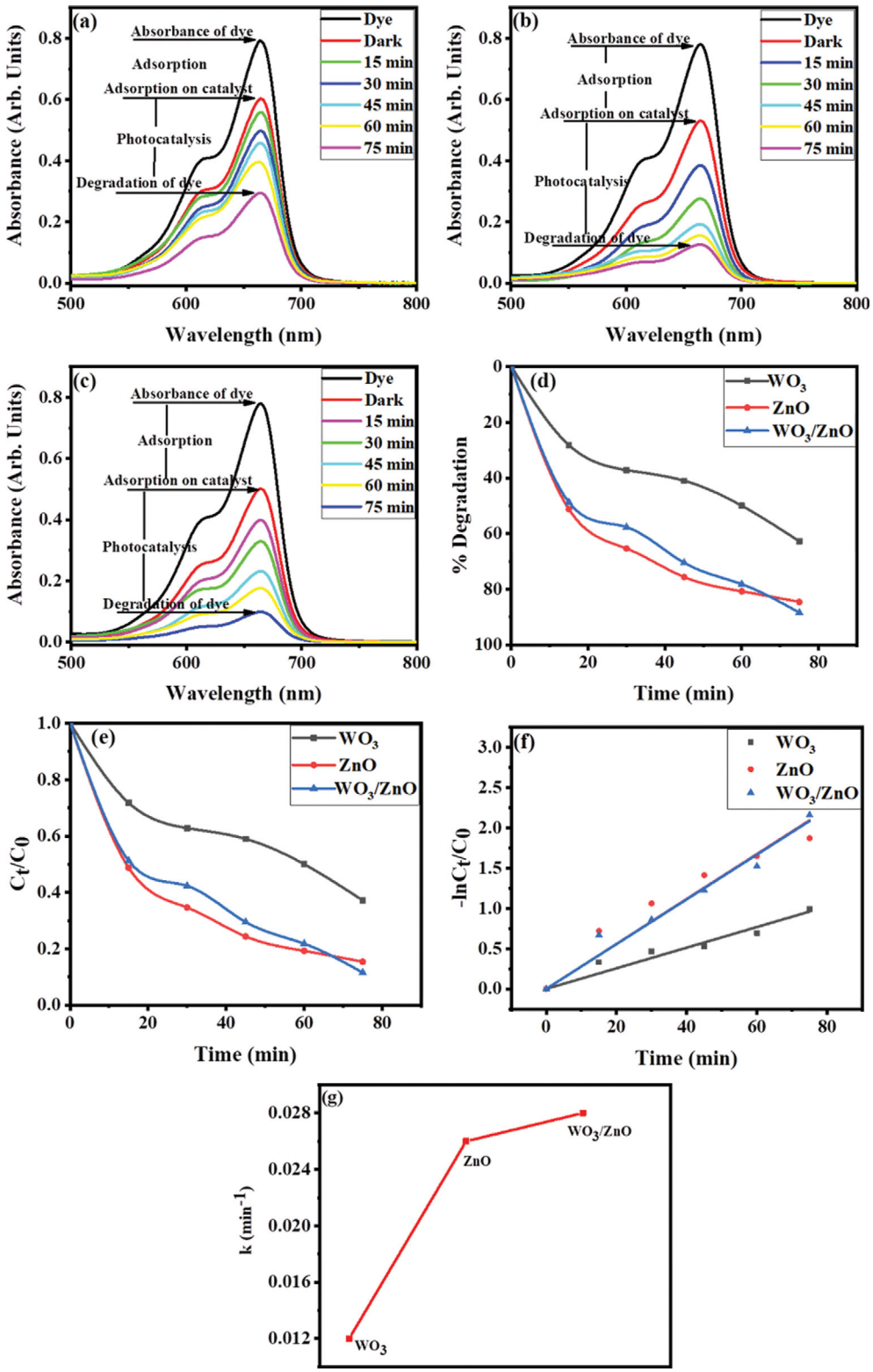

Fig. S2. Degradation spectra of methylene blue with WO_3, ZnO and their hetero-metallic oxide WO_3/ZnO using Iso-propyl alcohol as scavenger.

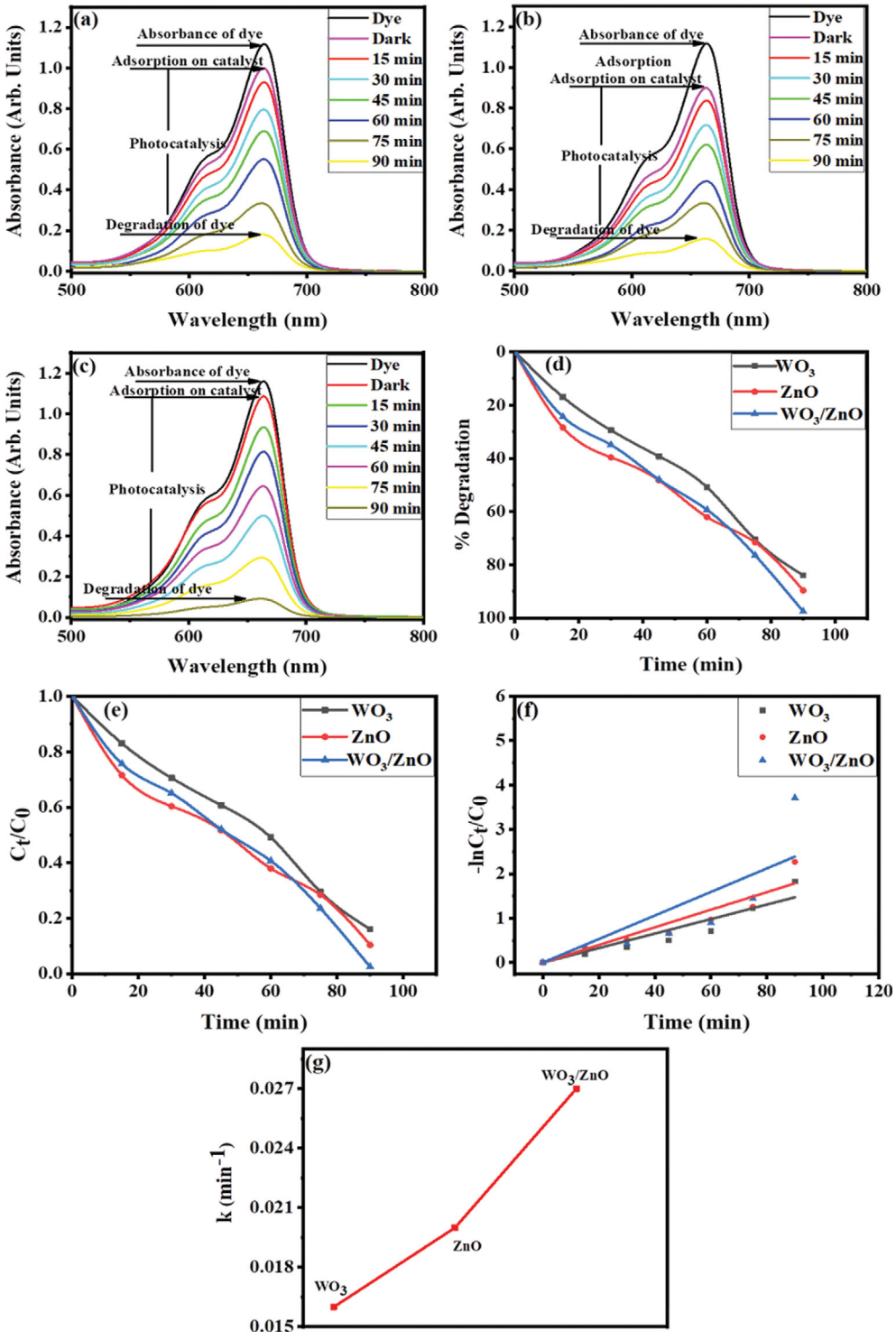

Fig. S3. Degradation spectra of methylene blue with WO_3, ZnO and their hetero-metallic oxide WO_3/ZnO using ascorbic acid as scavenger.

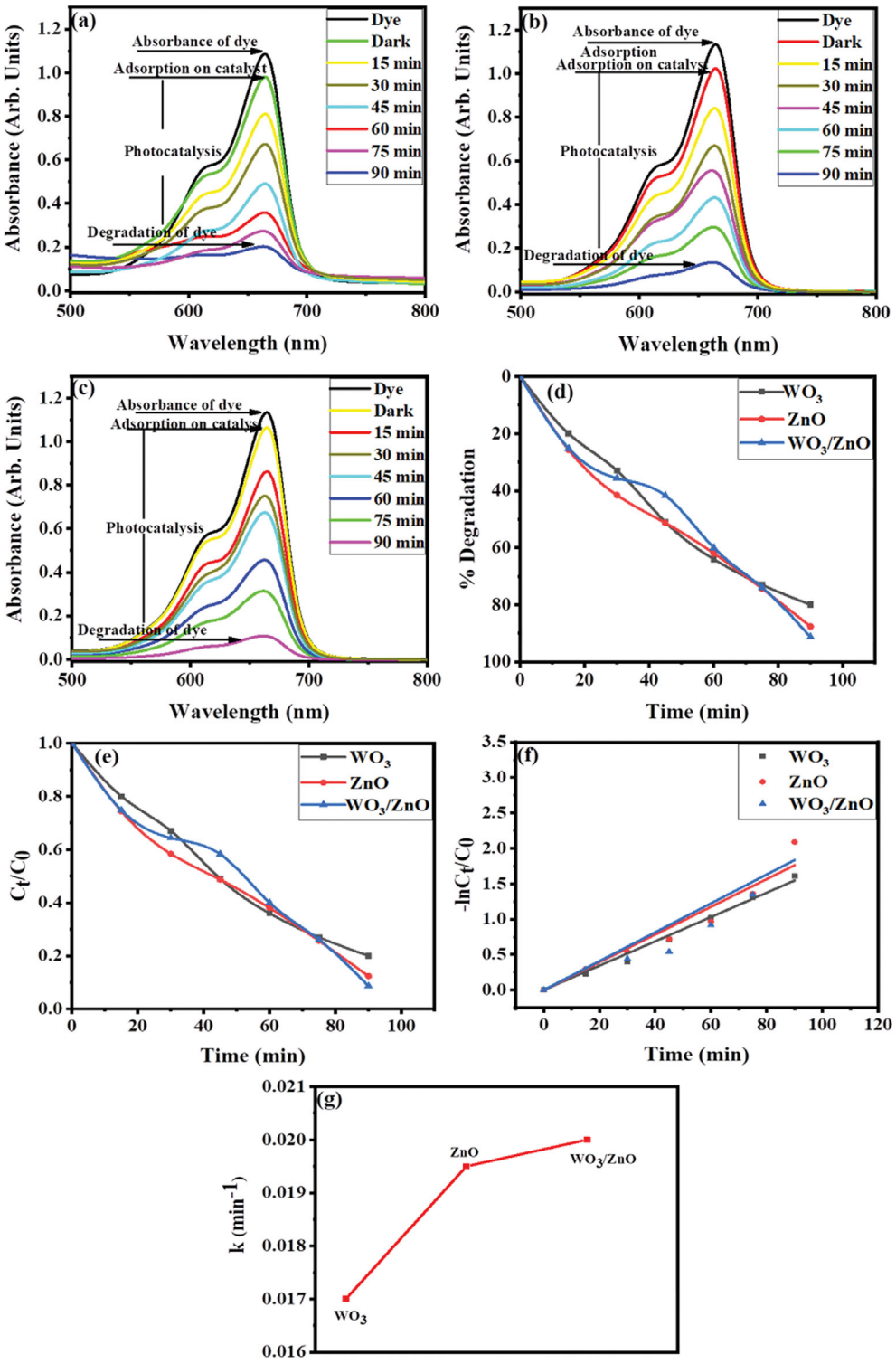

Fig. S4. Degradation spectra of methylene blue with WO_3, ZnO and their hetero-metallic oxide WO_3/ZnO respectively using $AgNO_3$ as scavenger.